Nanoscale

Accepted Manuscript

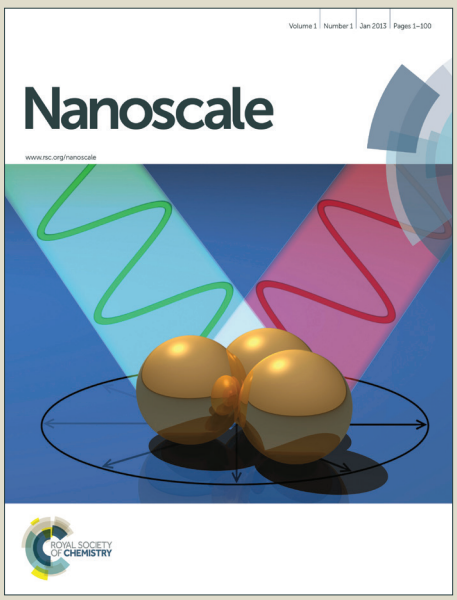

ROYAL SOCIETY OF CHEMISTRY

www.rsc.org/nanoscale

Hierarchical Interfaces Induce High-Dielectric –Permittivity of Nanocomposites Containing TiO_2@$BaTiO_3$ Nanofibers: Phase-Field Simulation and in-situ Observation of Electrical Breakdown by TEM

Xin Zhang[1], Weiwei Chen[1], Jianjun Wang[1], Yang Shen*[1], L. Gu[2], Yuanhua Lin[1], and Ce-Wen Nan*[1]

1 School of Materials Science and Engineering, State Key Lab of New Ceramics and Fine Processing, Tsinghua University Beijing, 100084, China.

2 *Chinese Academy of Science, Institute of Physics, Beijing National Lab of Condensed Matter Physics, POB 603, Beijing 100190, China.*

E-mail: shyang_mse@tsinghua.edu.cn; cwnan@tsinghua.edu.cn

Keywords: interface • topological structure • dielectric • nanocomposites

Abstract:

Interface issues are common and crucial in nanocomposites or nanohybrid systems since the interface area is enormous on the nanoscale. In the 0-3 polymer nanocomposites, in which nano-inclusions (0-dimension) are embedded in 3-dimensionally connected polymer matrix, enhanced dielectric permittivity could be induced by the interfacial polarization at the interfaces between the nano-inclusions and polymer matrix. In this contribution, we propose and demonstrate that the topological structure of the interface plays an equally important role as the area of interface in determining the dielectric polarization of polymer nanocomposites. TiO_2 nanofibers embedded with $BaTiO_3$ nanoparticles are prepared via electrospinning and then fused with polyvinyl difluoride (PVDF) into polymer nanocomposite films. Modulation of hierarchical interfaces are thus achieved in these nanocomposites. The confinement of these additional interfaces inside the TiO_2 nanofibers

leads to percolated networks formed by the interfacial regions. Dielectric permittivity of the polymer nanocomposites is thus enhanced by ~300% over the PVDF matrix at low fillers loading of 11 vol%. A phase-field simulation indicate that the enhanced dielectric permittivity could be attributed to the increased polarization in the percolated interfacial regions inside the TiO_2 nanofibers. The instantaneous electrical breakdown of the TiO_2@$BaTiO_3$ nanofibers by the in-situ transmission electron microscopy method further reveals the striking feature that the breakdown behavior of the nanofibers changes from semiconductive to metallic with the incorporation of insulating $BaTiO_3$ nanoparticles.

Introductions

Flexible polymer nanocomposites are critical in a number of applications in the modern information and electronic industry[1-3]. In these polymer nanocomposites, synergistic fusion of polymers and active nano-inclusions gives rise to superior thermal transportation performance[4], high electric conductivity or much enhanced dielectric polarization[5]. Interfacial issues between the polymers and nano-inclusions are most dominant in determining the performances of polymer nanocomposites. For instance, the Kapitza thermal resistance at the polymer/nano-inclusion interface seriously limit the maximal thermal conductivity that could be achieved in polymer nanocomposites even carbon nanotubes[6] or boron nitride[4] of super high thermal transportation properties are employed as nano-inclusions. Same interfacial effect also is present in the dielectric performance of polymer nanocomposites. Nano-inclusions of non-ferroelectric (TiO_2[7,8]), ferroelectric ($BaTiO_3$[9-11]), or paraelectric ($Ba_xSr_{1-x}TiO_3$[12]) have been introduced to improve the dielectric performance of polymer nanocomposites. Given the prominent differences in their intrinsic dielectric properties, these nano-inclusions induced very minor differences in the dielectric

behaviours of the polymer nanocomposites. The intrinsic dielectric responses of the nano-inclusions are overwhelmed by the dielectric behaviours of the interfacial regions.[13, 14]

In principle, dielectric behaviours in the interfacial regions are different from the nano-inclusions or polymer matrix, which could be attributed to additional interfacial polarization. Two mechanisms may be used to account for the interfacial polarization. The first is the enhanced ionic polarization and electronic polarization across the interface of which the dielectric enhancement has been investigated by first principle calculations at atomic level.[15,16] Such enhancement in dielectric permittivity is, however, restricted within only so few layers of atoms across the interface that it cannot improve the overall dielectric behaviour of the whole composite. The second mechanism is the field-induced polarization due to the mobile space charges, including impurities, electronics and holes, distributing in the interfacial regions according to the classic diffuse double-layer model.[17] The motion of charges in the diffuse layer under the applied electric field induces significant polarization, thus produce high dielectric permittivity. As the volume fraction of nano-inclusions increases close to the percolation threshold, the interfacial regions around the individual nano-inclusions overlap to form percolating paths for the mobile charges trapped within the diffuse layers. Motions of the mobile charges within the percolating paths through tunnelling then give rise to even much stronger space charge polarization.

In order to induce higher interfacial polarization hence higher dielectric permittivity, tremendous efforts have been made in preparing 0-3 type polymer nanocomposites with high loading of nano-inclusions. Yet, more interfacial imperfections, such as hole or voids, are also introduced in the interfacial regions at high loadings of nano-inclusions, resulting in increased dielectric loss, although some improvements might be made by modifing the interface between the fillers and the polymer matrix.[18,19] Ferroelectric nanofibers of large aspect ratio are thus employed as

nano-inclusions due to their larger dielectric dipolar moment, which lead to higher dielectric permittivity of polymer nanocomposites at lower volume fractions of nano-inclusions, as compared with their spherical counterparts. In this contribution, we propose and demonstrate that in addition to the interfaces between polymer and nanofibers, additional interfaces could be introduced from within the nanofibers by embedding $BaTiO_3$ nanoparticles inside the TiO_2 nanofibers (TO@BTO_nfs for short & Figure 1d). It is thus possible for us to manipulate the topological structure of interfaces for enhanced interfacial polarization. Our results indicate that, with optimal topological structure of interfaces, high dielectric permittivities of ~ 41 at low nanofiber loading of ~ 11 vol% could be achieved, which is an enhancement of ~ 300% over the polyvinylidene fluoride (PVDF) matrix. As shown in Figure 1, binary PVDF-based nanocomposites filled with TiO_2 nanofibers (TO_nfs for short and shown in Figure 1a) or $BaTiO_3$ nanoparticles (BTO_nps & Figure 1b), as well as ternary nanocomposites simultaneously filled with TO_nfs and BTO_nps (Figure 1c), are also prepared with their dielectric behaviour investigated. The enhanced dielectric permittivity could not be attributed soley to the increase in the area of interfaces. Instead, a phase-field simulation suggests that the confinement of internal interfaces within the nanofibers, as shown in Fig. 1d, leads to percolated interfacial regions and give rise to significantly increased polarization of the nanofibers hence much higher dielectric permittivity.

Experimental

Synthesis of BTO@TO_nfs and pure TO_nfs via electrospinning.

All the chemicals were purchased from China National Chemicals if Corporation Ltd. if not otherwise specified. BTO@TO_nfs with average diameter around 300nm were synthesized via electrospinning. Precursor sols were prepared by dissolving tetrabutyl titanate into ethanol. Then $BaTiO_3$ nanoparticles were added into prepared sol and thoroughly mixed to form stable sol for

electrospinning. Poly(vinyl pyrrolidone) was used to adjust the viscosity of precursor sol to the optimum value for the following electrospinning. The sol was then transferred into a syringe and electrospinning was carried out with electric field of 1.3KV cm^{-1}. The as-electrospun composites fibers were calcined at 500^{o}C for the pyrolysis of organic constituents. TO_nfs were also synthesized with identical process without adding BTO_nps.

Surface modification of fillers with dopamine.

The prepared BTO_nps, TO_nfs, TO@BTO_nfs were dispersed into dopamine hydrochloride (99%, Alfa Aesar) aqueous solution with a concentration of 0.01 mol L^{-1} respectively and stirred for 10 h at 60^{o}C, then separated from suspensions by centrifugation and finally dried for 6h at 70^{o}C. The coated layer of dopamine were observed by High-resolution transmission electron microscopy (HRTEM, JEOL2011) and further characterized by Transformed Infra-Red spectroscopy (FTIR, Nicolet 6700).

Preparation of polymer nanocomposites films.

Polyvinylidene fluoride were thoroughly dissolved in N,N-dimethylformamide (DMF), followed by the dispersion of the nano-inclusions in the solution with ultrasonication. Polymer nanocomposite films were then cast from the solutions with a Laboratory Casting Equipment (LY-150-1, Beijing Orient Sun-Tec Company, Ltd). After being dried at 50^{o}C for 10 h, the final polymer nanocomposite films are ~ 16 μm in thickness. Morphologies of TO_nfs, TO@BTO_nfs and films were characterized by scanning electron microscopy (SEM, Hitachi S-4500), high-resolution transmission electron microscopy (HRTEM, JEOL2011) and Fourier Transformed Infra-Red spectroscopy (FTIR, Nicolet 6700). The contents of the nano-inclusions in the final polymer nanocomposites are determined by thermal gravimetric analysis (TGA, TGA/DSC1, Metter-Toledo, Switzerland).

Measurement of dielectric properties.

Cu electrodes with diameter of 3 mm were coated on both sides of the films by evaporation for the dielectric measurement. Dielectric permittivity and dielectric loss were measured with a HP 4294A precision impedance analyzer (Agilent) at room temperature.

In-situ observation of electrical breakdown by TEM

All in situ TEM observation of breakdown behaviors were conducted with a FEI Tecnai F20 STM. Well dispersed TO@BTO_nfs were glued to an Au wire by silver paste, and the fiber-attached Au wire was inserted into a TEM-scanning tunneling microscopy holder (Nanofactory *in-situ* holder,ST 1000), which enables the connection and conduction between the nanofiber and electrodes. The bias applied for the electrical breakdown measurements was increased at a ramping rate of 2V/s.

Results & Discussions

Morphology of TiO_2@$BaTiO_3$ Nanofibers

The TiO_2 composite nanofibers embedded with $BaTiO_3$ nanoparticles (TO@BTO_nfs for short, here after) are prepared via a facile electrospinning process. Briefly, $BaTiO_3$ nanoparticles of ~ 50 nm in diameter are dispersed in tetrabutyl titanate as precursors for electrospinning. The as-prepared composite nanofibers are then subjected to calcination at 500^{o}C for the pyrolysis of organic constituents, giving rise to well crystallized anatase TiO_2 nanofibers of tetragonal phase (see the XRD patterns shown Figure 2). TO@BTO_nfs with $BaTiO_3$/TiO_2 ratio of 1:1 and 1:2 in volume are prepared. Scanning electron microscopy (SEM) and Transmission electron microscopy (TEM) images, as shown in a1 and a3 in the inset of Figure 2 respectively, indicate that BTO_nps are connected to form clusters inside the TO_nfs, which could also be observed in the dark-field TEM

image of the TO@BTO_nfs (a2 in the inset of Figure 2). After ultrasonication process during the preparation of polymer nanocomposites, the as-calcined TO@ BTO_nfs are broken into short fibers with the aspect ratios of 15 to 20. Pure TO_nfs of the same diameter and aspect ratios were also prepared with the identical processing method. (see Figure S2 in the supporting information). Thin layers of dopamine were coated on all the nano-inclusions to facilitate their dispersion in PVDF matrix, as shown in Figure S3 in the supporting information. Homogeneous dispersions of all nano-inclusions in the PVDF matrix are achieved in these nanocomposites. (see Figure S4 in the supporting information) Also could be observed in Figure S4 is the orientation of nanofibers in the in-plane directions of the nanocomposite films, which is due to the large aspect ratios of the nanofibers and has important implications for the dielectric behaviors of these nanocomposites.

Dielectric performances of the PVDF-based nanocomposites

The introduction of the three types of nano-inclusions could all lead to enhancement in dielectric permittivity in the PVDF-based nanocomposites, as shown in Figure 3. Two striking features could be readily observed from the variation of dielectric permittivity with the volume fraction of nano-inclusions (Figure 3a). i) The dielectric permittivity of the polymer nanocomposites filled the TO@BTO_nfs is consistently higher than the polymer nanocomposites filled with either nano-inclusions at all volume fractions. Notably, the most significant enhancement is achieved at 11.4 vol% of TO@BTO_nfs, i.e., from ~ 11 for PVDF to ~ 41 in TO@BTO_nfs/PVDF nanocomposites at 100 Hz, which is an enhancement of ~ 300%; ii) Mild enhancement in dielectric permittivity is observed in the ternary polymer nanocomposites co-filled with BTO_nps and TO_nfs, which lies right in between the BTO_np/PVDF and TO_nf/PVDF binary nanocomposites. It is of interest to note that the high dielectric permittivity value of ~ 41 is comparable to the highest reported values, [17, 20-23] yet is achieved at the lowest volume fraction of

nano-inclusions. In similar nanocomposites based on PVDF or its copolymers[11,24], at least over 35 vol% of $BaTiO_3$ nanoparticles were needed to obtain the same dielectric permittivity, which is over three times the amount of nano-inclusions employed in our nanocomposites. Moreover, the enhancement in dielectric permittivity is not achieved at the expense of the much increased dielectric loss, as shown in the frequency relaxation of dielectric permittivity (Figure 3b). As seen, all the polymer nanocomposites are still highly insulating, as evidenced by the very minor increase in dielectric loss at lower frequencies. At 10 MHz, the dielectric loss is even slightly lower for the polymer nanocomposites than for the PVDF matrix.

The favourable effects of hierarchical interfaces within the TO@BTO_nfs on the dielectric performance are further distinguished in Figure 3c. With the fixed sum volume fraction of 11.4 vol% in the ternary polymer nanocomposites co-filled with BTO_nps and TO_nfs, very minor change in dielectric permittivity is observed as the BTO:TO ratio increases from 1:2 to 1:1. While much more prominent increase in dielectric permittivity is achieved in the TO@BTO_nfs/PVDF nanocomposites, as shown in Figure 3c.

Variation of dielectric permittivity with specific interfacial area

For further clarification of the role of interface, the specific interfacial area, i.e., the area of interface per unit volume (in m^2/cm^3), of the polymer nanocomposites is determined from the dimensions and volume fractions of the nano-inclusions. The dielectric permittivity of each polymer nanocomposites is then plotted as a function of their specific interfacial area, as show in Figure 4. There are two striking features to the data when presented this way. First, as the specific interfacial area increases from ~ 1.1 m^2/cm^3 for the TO_nf/PVDF (a-type) to ~ 13.9 m^2/cm^3 for the BTO_np/PVDF (b-type), the dielectric permittivity of the polymer nanocomposites increases mildly from ~ 27 to ~ 31. The mechanism that larger interfacial area leads to higher dielectric permittivity

still holds for the binary nanocomposites of a-type and b-type as well as for the c-type nanocomposites. Second, with the same specific interfacial area of ~ 7.9 m^2/cm^3 for both the TO@BTO_nfs/PVDF (d-type) and the ternary nanocomposites co-filled with BTO_nps and TO_nfs (c-type), the dielectric permittivity increases by ~ 41 %, i.e., from ~ 29 for c-type nanocomposites to ~ 41 for d-type nanocomposites, as indicated by the arrow in Figure 4. The implication of the abrupt increase in dielectric permittivity at the same specific interfacial area is that there might be other mechanisms involved in determining the interfacial polarization, other than simply increasing the area of interfaces. The reasons are two folds: i) The proportion by which the dielectric permittivity increases with the specific interfacial area is so limited that the increase of specific interfacial area by ten folds (from ~ 1.1 m^2/cm^3 for the TO_nf/PVDF to ~ 13.9 m^2/cm^3 for the BTO_np/PVDF nanocomposites) only leads to minor enhancement in dielectric permittivity by ~1.5%. ii) The confinement of BTO_nps inside the TO_nfs gives rise to much more pronounced increase in dielectric permittivity from c-type to d-type nanocomposites, even the specific interfacial area remains the same for the two nanocomposites.

Polarization and electric field distribution simulated by the phase-field model

The most prominent difference in microstructural morphology between c-type and d-type nanocomposites is the topological structure of the interfaces. As shown in a2 of the inset in Fig. 2, the BTO_nps form clusters inside the TO_nfs which leads to percolated interfacial region. In order to further explore the effects of the topological structure of interface on the dielectric enhancement in the nanocomposites from the microscopic point of view, we employ the Spectral Iterative Perturbation Method (SIPM) [25] to solve the electrostatic equilibrium equations for the above discussed four types of structures and hence obtain the polarization distributions in the nanocomposites. In the four types of nanocomposites discussed, each nanocomposite can be divided

into the following phases: BTO particle phase α (use α as the order parameter to define the BTO particle phase, α =1 represents the BTO particle phase and whereas not α =0), TO fibre phase β, PVDF matrix phase γ, BTO-PVDF interfacial phase η, TO-PVDF interfacial phase ξ, and BTO-TO interfacial phase ω, and hence the phase dependent dielectric constant can be written as

$$\boldsymbol{\kappa}(\mathbf{r}) = \boldsymbol{\kappa}^{\alpha}\alpha(\mathbf{r}) + \boldsymbol{\kappa}^{\beta}\beta(\mathbf{r}) + \boldsymbol{\kappa}^{\gamma}\gamma(\mathbf{r}) + \boldsymbol{\kappa}^{\eta}\eta(\mathbf{r}) + \boldsymbol{\kappa}^{\xi}\xi(\mathbf{r}) + \boldsymbol{\kappa}^{\omega}\omega(\mathbf{r}). \quad (1)$$

The electric displacement $\mathbf{D}(\mathbf{r})$ in each composite system can be obtained by

$$\mathbf{D}(\mathbf{r})=\varepsilon_0\boldsymbol{\kappa}(\mathbf{r})\mathbf{E}(\mathbf{r})+\mathbf{P}^{\mathrm{S}}(\mathbf{r}), \quad (2)$$

Where ε_0 is the dielectric permittivity of the vacuum, $\boldsymbol{\kappa}(\mathbf{r})$ the phase dependent relative dielectric constant, $\mathbf{E}(\mathbf{r})$ the total electric field distribution, and $\mathbf{P}^{\mathrm{S}}(\mathbf{r})$ the phase dependent spontaneous polarization of the composites. Using the SIPM method to solve the electrostatic equilibrium equation

$$\nabla\cdot\mathbf{D}(\mathbf{r})=0, \quad (3)$$

We can obtain the spatially total electric field distribution $\mathbf{E}(\mathbf{r})$. The total polarization distribution is given by

$$\mathbf{P}(\mathbf{r})=\varepsilon_0(\boldsymbol{\kappa}(\mathbf{r})-\boldsymbol{\delta})\cdot\mathbf{E}(\mathbf{r})+\mathbf{P}^{\mathrm{S}}(\mathbf{r}) \quad (4)$$

with $\boldsymbol{\delta}$ the Dirac delta function.

The distributions of interfacial polarization are simulated in the configuration that the majority of the nanofibers is oriented in the in-plane directions of the polymer nanocomposite films as evidenced by the SEM images of the polymer nanocomposites (see Figure S4 in the supporting information). The polarization thus simulated for the four types of nanocomposites with the same

nano-inclusion loading of 11.4 vol% are shown in Figure 4, alongside their corresponding dielectric permittivity. It is of interest to note that equal amount of BTO_nps are present in both c-type and d-type nanocomposites. Yet, being confined within the TO_nfs, the BTO_nps in the d-type nanocomposites are more easily connected to form percolated interfacial regions and induce much enhanced interfacial polarization along the external electric field direction (as indicated by the intensified red interfacial regions in d of Figure 4). In contrast, in the b-type nanocomposites, the amount of BTO_nps is twice as many as that in d-type nanocomposites. However, being randomly dispersed in the PVDF matrix, the BTO_nps have smaller probability of forming percolated interfacial networks, although the specific interface area in b-type nanocomposites (~ 13.9 m^2/cm^3) is almost two times larger than that in in d-type nanocomposites (~ 7.9 m^2/cm^3). The enhancement in the overall interfacial polarization is thus less significant for b-type nanocomposites.

The implication of the much enhanced interfacial polarization is that the relative dielectric permittivity is also substantially increased for the TO@BTO_nfs with BTO:TO ratio of 1:1, which then leads to larger dielectric mismatch between the PVDF matrix and the TO@BTO_nfs. As a result, significant electric field concentration in the PVDF matrix is induced, as indicated by the intensified red area in between the two neighbouring TO@BTO_nfs in Figure 5d2. In contrast, electric field is only concentrated in the PVDF matrix between two neighbouring BTO_nps (Figure 5b&c), while TO_nfs of low dielectric permittivity only induce minor electric field concentration which is mostly observed at the tips of the nanofibers (Figure 5a). In the TO@BTO_nfs with BTO:TO ratio of 1:2, percolating paths of interfacial regions could not be established due to the low content of BTO_nps and hence minor enhancement of interfacial polarization is induced, as shown in Figure S9 in the supporting information. As a result, less significant electric field concentration

could only be observed at the tips of the TO@BTO_nfs (Figure 5d1), which is very similar to the scenario of TO_nfs/PVDF nanocomposites.

Both the dielectric characterization and the phase-field simulation suggest that the percolated interfacial regions in the TO@BTO_nfs substantially increase the dielectric permittivity of these nanofibers. In fact, similar enhancement of dielectric permittivity has also been observed in the polymer nanocomposites filled with $BaTiO_3$ nanoparticles of which a thin layer of TiO_2 is coated. As the volume fraction of the core-shell $BaTiO_3$@TiO_2 nanoparticles increases to ~ 50 vol%, the TiO_2 interface layers form percolating paths for the charges accumulated within the interfacial regions, giving rise to much enhanced dielectric permittivity of ~ 120.[26] As a result of the increased polarization of the space charges, the electrical breakdown strength of these polymer nanocomposites is substantially decreased. It is thus of interest to characterize the electrical breakdown of the TO@BTO_nfs as the BTO:TO ratio varies from 1:2 to 1:1, because the TO@BTO_nfs may be considered as nanocomposites analogous to those polymer nanocomposites containing core-shell $BaTiO_3$@TiO_2 nanoparticles.

Direct observation of electrical breakdown of TO@BTO_nfs by *in-situ* TEM method

The FEI Tecnai F20 STEM and nanofactory in-situ TEM-scanning tunnelling microscopy holder are used for applying DC bias on the TO@BTO_nfs. The whole setup is schematically drawn in Figure 6. (The experimental procedures are described in detail in the supporting information) DC bias were continuously applied to the TO@BTO_nfs with BTO:TO ratio of 1:2 (Figure 6a) or 1:1 (Figure 6b) at a ramping rate of 2V/s. The dynamic breakdown processes are also recorded in the videos in supporting information. With the increasing DC voltage, the nanofibers with different BTO:TO ratios break at different maximal voltage, i.e., 30 V for the BTO:TO ratio of 1:2 and 8 V for 1:1. Given the same lengths of the two nanofibers (~ 4 μm as measured from Figure

6a1 & 6b1), the electrical breakdown fields determined for the two nanofibers are substantially different, i.e., ~ 7.5 kV/mm for nanofibers with BTO:TO ratio of 1:2 and ~ 2 kV/mm for 1:1. It is also worth noting that the TO@BTO_nfs with BTO:TO ratio of 1:2 break near the middle (Figure 6a2), while the electrical breakdown initiates at the end of the nanofiber with BTO:TO ratio of 1:1 (Figure 6b2). The implication of the different breakdown point is that the TO@BTO_nfs with different amount of BTO_nps may be quite different in their electrical properties.

In principle, two mechanisms are involved in the electrical breakdown of nanofibers, or nanowires, i.e., electro-breakdown and thermo-breakdown, which depend mainly on the electrical and thermal properties of materials. Specifically, semiconductive nanofibers are thermally broken by the Joule heating, while the electrical breakdown of metallic nanofibers is caused by the stress accumulated at the two ends induced by electromigration.[27] The tendency of thermal heating breakdown or electrobreakdown of a certain nanofibers could be estimated as:[27]

$$\frac{\sigma/Z*^2}{k} \sim \frac{8e^2\Delta T}{\Omega^2\Delta s^2} \qquad (5).$$

Where σ and κ are the electrical and thermal conductivity of the nanofiber respectively, while Z* is the effective charge. By substituting general parameters for materials in eq. 5, one concise relationship, as $\sigma/\kappa Z*^2 = 2 \times 10^4$ K/ΩW, is then derived and could be employed as a qualitative estimation for the different breakdown mechanisms.[27] It should be noted that this relationship is derived for single crystalline or nearly single crystalline nanofibers, where neither the heat dissipation barriers or electron scattering centers induced by the interfaces are considered. Nevertheless, it may still shed some light on the analysis of the electrical breakdown behaviour of our TO@BTO_nfs. The thermal conductivities of anatase TiO_2 and cubic $BaTiO_3$ lie in the same range of 2 ~ 3 W/mK,[28] while their electrical conductivities are substantially different, i.e., 10^{-3} S/m for TiO_2 and 10^{-7} S/m for $BaTiO_3$.[29] The $\sigma/\kappa Z*^2$ values of TiO_2 and $BaTiO_3$ thus determined are

much smaller than 2 x 10^4 K/ΩW, indicating that thermo-breakdown is the primary mechanism for pure TiO_2 nanofibers as well as for $BaTiO_3$. Indeed, the TO@BTO_nfs with BTO:TO ratio of 1:2 was broken in the middle point of the nanofiber (as shown in Figure 6a2), which is indicative of thermo-breakdown. Yet, different breakdown behaviour is observed for the TO@BTO_nfs with BTO:TO ratio of 1:1. Instead of being broken in the middle by thermally heating, as one may expect from the higher volume fraction of the more insulating $BaTiO_3$ nanoparticles, the TO@BTO_nfs with BTO:TO ratio of 1:1 break in a more intensive process which initiates at the end of the nanofiber close to the electrode. The dynamic breakdown process (as recorded in the video of supporting information) further reveals a sudden breakdown of the nanofiber, which is very similar to the stress-induced electro-breakdown caused by electromigration. As the volume fraction of $BaTiO_3$ nanoparticles increases, the networks of the interfacial regions provide percolating paths for the charges in the interfacial regions. Under DC bias, charges in the interfacial regions migrate along the external electric field and accumulate at the end of the nanofibers to build very high depolarization electric field, resulting in significant amount of stress. In fact, the stress was so high that the TO@BTO_nf broke almost instantaneously, as shown in the video of supporting information. The percolated interfaces increase the overall polarization the TO@BTO_nfs with BTO:TO ratio of 1:1 and substantially change their electrical breakdown behaviour, which agree well with the results of phase-field simulations.

Conclusions

In summary, significant enhancement in dielectric permittivity is achieved with the modulation of hierarchical interfaces in polymer nanocomposites by employing TO@BTO_nfs. In the TO@BTO_nfs, the embedded BTO_nps are confined within the TO_nfs to form interconnected networks of interfacial regions. A phase field simulation confirmed that much enhanced interfacial

polarization is thus induced by the motion of space charges within these percolating paths, which then gives rise to high dielectric permittivity of the polymer nanocomposites. The enhanced interfacial polarization is so significant that it even change the electrical breakdown behaviour of the TO@BTO_nfs from being semiconductor to more like metal, as indicated by the *in-situ* observation of electrical breakdown of the TO@BTO_nfs. Our results suggest that the topological structure of interfaces between nano-inclusions and polymer plays equally important roles, as the intrinsic dielectric property of the nano-inclusions, in determining the dielectric performance of the polymer nanocomposites. This approach may pave the avenue for designing and achieving high-κ polymer nanocomposites with rather low loading of nano-inclusions and hence greater flexibility. Plus, the modulation of topological structure of interfaces may also be extended in other hybrid systems where interfaces are crucial.

Acknowledgements

This work was supported by the NSF of China (Grant Nos. 51102142, 51222204), Specialized Research Fund for the Doctoral Program of Higher Education (Grant No.20110002120004), the Foundation for the Authors of National Excellent Doctoral Dissertations of China (Grant No.: 201144), Beijing Nova Program (Grant No.: XX2013037) and Tsinghua University (Grant No.20121087925)

References

1 W. Jillek and W. K. C. Yung, Int. ***J Adv. Manuf. Technol***. **2005**, *25*, 350-360.

2 Z.-M. Dang, J.-K. Yuan, S.-H. Yao, R.-J. Liao, ***Adv. Mater.*** **2013**, 25, 6334-6365

3 J. Biggs, K. Danielmeier, J. Hitzbleck, J. Krause, T. Kridl, S. Nowak et.al., ***Angew. Chem. Int. Ed.*** **2013**, *52*, 9409-9421.

4 W. L. Song, P. Wang, L. Cao, A. Anderson, M. J. Meziani, A.J. Farr and Y. P. Sun, ***Angew. Chem. Int. Ed.*** **2012**, *51*, 6498-6501.

5 M. S. Wang, J. L. Zhu, W. L. Zhu, B. Zhu, J. Liu, X. H. Zhu et.al., ***Angew. Chem. Int. Ed.*** **2012**, *51*, 9123

6 C. W. Nan and Z. Shi, ***Chem. Phys. Lett.*** **2003**, *375*, 666-689.

7 T.-I. Yang and P. Kofinas, ***Polymer.*** **2007**, *483*, 791-798.

8 J.-J. Li, S.T. Seok, B.-J. Chu, F. Dogan, Q.-M. Zhang, Q. Wang, ***Adv. Mater.*** **2009**, *21,* 217-221.

9 P. Kim, S. C. Jones, P. J. Hotchkiss, J. N. Haddock, B. Kippelen, S. R. Marder, J.W. Perry, ***Adv. Mater.*** **2007**, *19*, 1001-1005.

10 H. M. Jung, J.-H. Kang, S. Y. Yang, J. C. Won, Y. S. Kim, ***Chem. Mater.*** **2009**, *22*, 450-456.

11 (a) P. Kim, N. M. Doss, J. P. Tillotson, P. J. Hotchkiss, M.-J. Pan, S. R. Marder, J.-Y. Li, J. P. Calame, J. W. Perry, ***ACS Nano.*** **2009**, *3*, 2581-2592. (b) K. Yang, X. Y. Huang, Y. H. Huang, L. Y. Xie, P. K. Jiang, ***Chem. Mater.*** **2013**, 25, 2327-2338. (c) L. Y. Xie, X. Y. Huang, Y. H. Huang, K. Yang, P. K. Jiang, ***J. Phys. Chem. C***, 2013, 117, 22525-22537

12 H.-X. Tang, H. A. Sodano, ***Nano Lett.*** **2013**, *13*, 1373-1379.

13 T. Tanaka, M. Kozako, N. Fuse, Y. Ohki, ***IEEE Trans. Dielectr. Electr. Insul.*** **2005**, 12, 669-681

14S. Siddabattuni, T. P. Schuman, F. Dogan, ***ACS Appl. Mater.Interface***. 2013, 5, 1917-1927.

15 F. Giustino, A. Pasquarello, ***Phys. Rev. B.* 2005**, 71, 144104

16 L.-P. Yu, V. Ranjan, M. B. Nardelli, J. Bernholc, ***Phys. Rev. B.* 2009**, 80, 165432

17 T. J. Lewis, ***IEEE Trans. Dielectr. Electr. Insul.* 2004**, 11, 739-753.

18 L. Gao, J. J. He, J. H, Y. Li, ***J. Phys. Chem. C***. 2014, 118, 831-838

19 M. Rahimabady, M. S. Mirshekarloo, K. Yao, L. Lu, ***Phys. Chem. Chem. Phys.*** 2013, 15, 16242

20 Z.-M. Dang, H.-Y. Wang, Y.-H. Zhang, J.-Q. Qi, ***Macromol. Rapid Commun***.2005, 26, 1185-1189

21 S.-F.Wang, Y.-R. Wang, K.-C. Cheng, Y.-P. Hsaio, ***Ceram. Int.*** 2009, 35, 265 -269

22 Z. M. Dang, H.-Y. Wang, H.-P. Xu, ***Appl. Phys. Lett.*** 2006, 89, 112902

23 H. M. Jung, J.H. Kang, S.Y. Yang, J.C. Won, and Y. S. Kim, ***Chem. Mater.*** 2010, 22, 450-456

24 J. Li, J. Claude, L. E. Norena-Franco, S. I. Seok, Q. Wang, ***Chem. Mater.*** 2008, 20, 6304-6306

25 J. J. Wang, X.Q. Ma, Q. Li, J. Britson, L.-Q. Chen, ***Acta Mater.* 2013**. 61,7591-7603.

26 M. Rahimabady, M. S. Mirshekarloo, K. Yao, and L. Lu, ***Phys. Chem. Chem. Phys.*** 2013, 15, 16242-16248

27 J. Zhao, H. Y. Sun, S. Dai, Y. Wang, and J. Zhu, ***Nano Lett.*** 2011, 11, 4647-4651

28 R. Z. Zhang, X. Y. Hu, P. Guo, and C. L. Wang, ***Physica B.*** 2012, 407, 1114-1118

29 I. A. Belasco-Davalos, A. Ruediger, J. J. Cruz-Rivera, C. Gomez-Yanez, ***J. Alloy. & Comp.*** 2013, 581, 56-58

Figure Captions:

Figure 1 Schematic illustrations of (a) TO_nf/PVDF nanocomposites, (b) BTO_np/PVDF nanocomposites, (c) nanocomposites co-filled with TO_nf and BTO_nf, and (d) nanocomposites filled with TO@BTO_nfs. Also superimposed is the distribution of dielectric permittivity among different regions in the nanocomposites. The enhanced interfacial polarization is indicated by the abrupt increase in dielectric permittivity in the interfacial regions. The interfacial region in (b) is magnified to show the structure of the diffuse electronic double layer.

Figure 2 XRD patterns of the TO@BTO_nfs with BTO:TO ratios of 1:1. The diffraction peaks are assigned to perovskite $BaTiO_3$ of cubic phase (solid square in green) and to anatase TiO_2 of tetragonal phase (solid circle in yellow). Also shown are (a1) SEM image, (a2) mapping image, and (a3) TEM image of the TO@BTO_nfs with BTO:TO ratios of 1:1.

Figure 3 (a) Variations of dielectric permittivity with the volume fraction of nano-inclusions in four types of nanocomposites; (b) The dependences of dielectric permittivity (solid) and dielectric loss (open) on frequency for four nanocomposites with the same nano-inclusion volume fraction of 11.4 vol.%; (c) The dependences of dielectric permittivity on frequency for c (open symbols) and d (solid symbols) type nanocomposites with different BTO:TO ratios.

Figure 4 Variations of dielectric permittivity with the Specific Interface Area of nano-inclusions in four types of nanocomposites. The increase of dielectric permittivity of nanocomposites filled with TO@BTO_nfs (BTO:TO ratio of 1:2 and 1:1) are highlighted in red square. The abrupt increase of dielectric permittivity from c type to d type nanocomposites at the same specific interfacial area is indicated by the red arrow. Alongside each nanocomposites is the distribution of interfacial polarization simulated for the corresponding nanocomposite. The phase field model employed in the simulation is described in detail in the text.

Figure 5 The distribution of electric field strength simulated for the (a) PVDF/TO_nfs, (b) PVDF/BTO_nps, (c1) PVDF/BTO_nps/TO_nfs with volume ratio of BTO:TO = 1:2, (c2)

PVDF/BTO_nps/TO_nfs with volume ratio of BTO:TO = 1:1, (d1)PVDF/TO@BTO_nfs with volume ratio of BTO:TO = 1:2, (d2)PVDF/TO@BTO_nfs with volume ratio of BTO:TO = 1:1.

Figure 6 TEM images for the TO@BTO_nfs with BTO:TO ratio of (a) 1:2 and (b) 1:1 before (a1 & b1) and after (a2 & b2) the breakdown measurements. The broken area is better distinguished in the magnified images (a3 & b3). Also presented is the schematic graph of the in-situ TEM-STM setup.

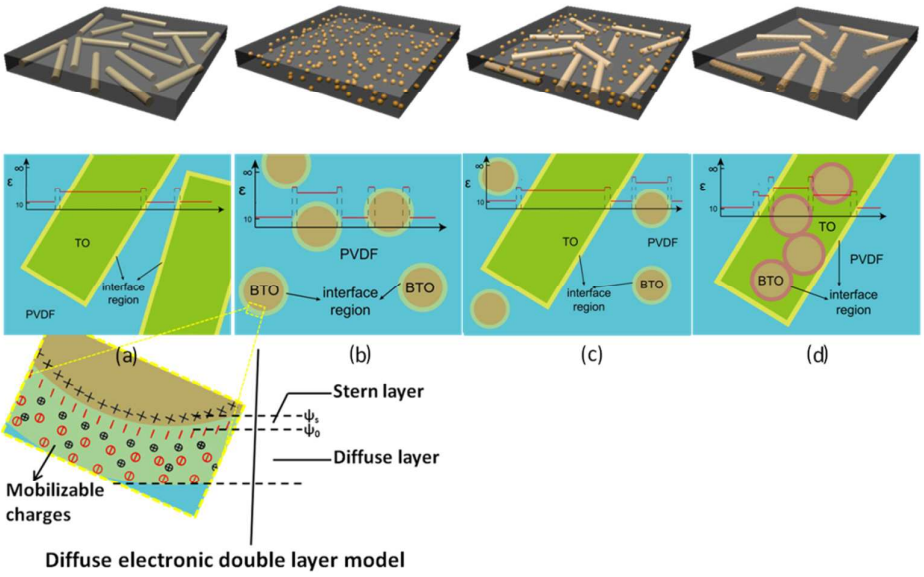

Figure 1

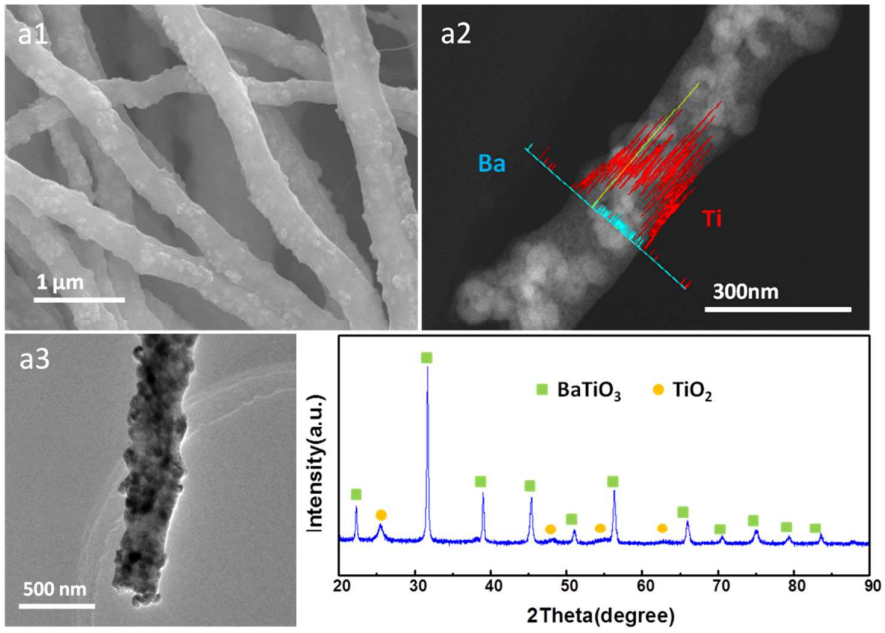

Figure 2

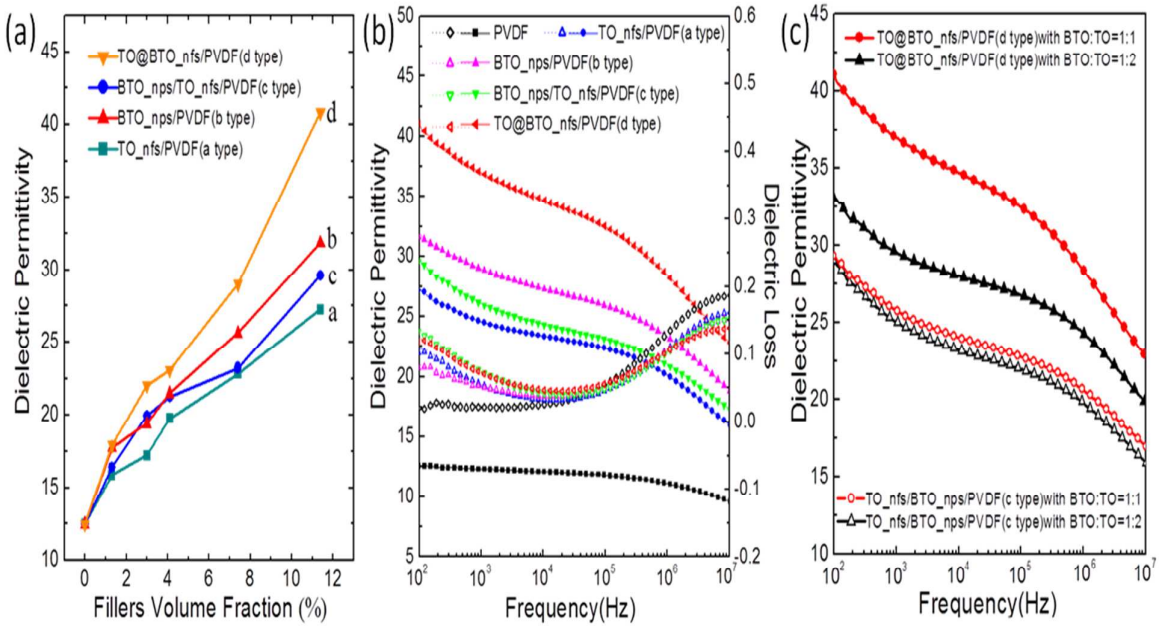

Figure 3

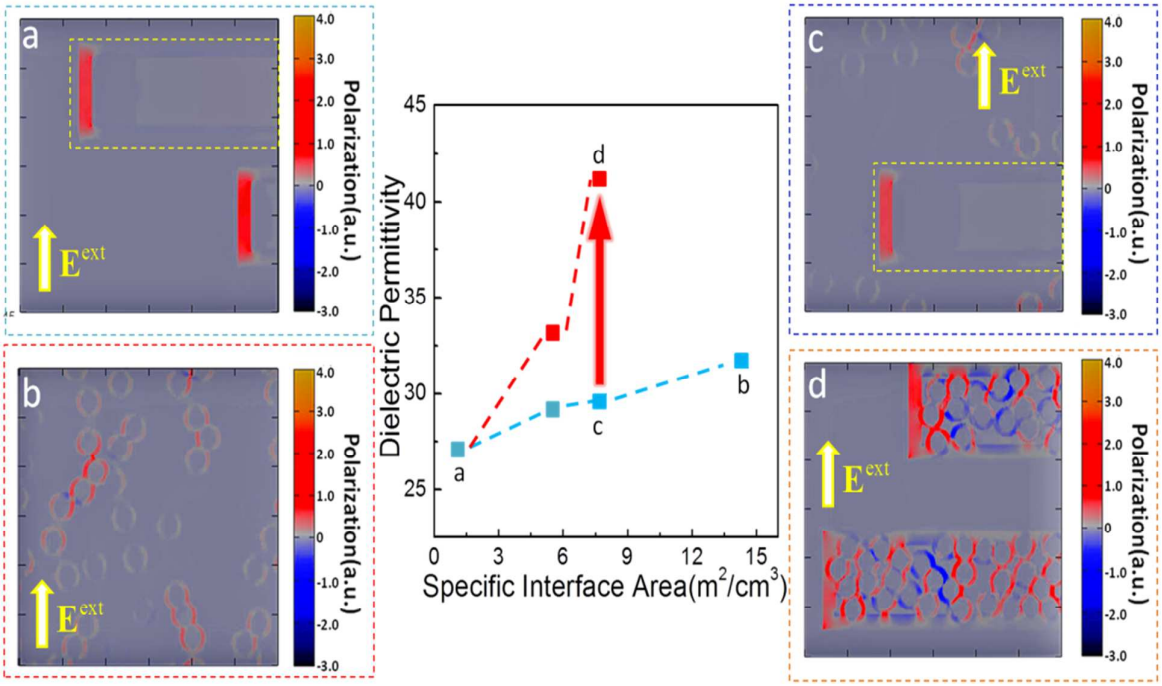

Figure 4

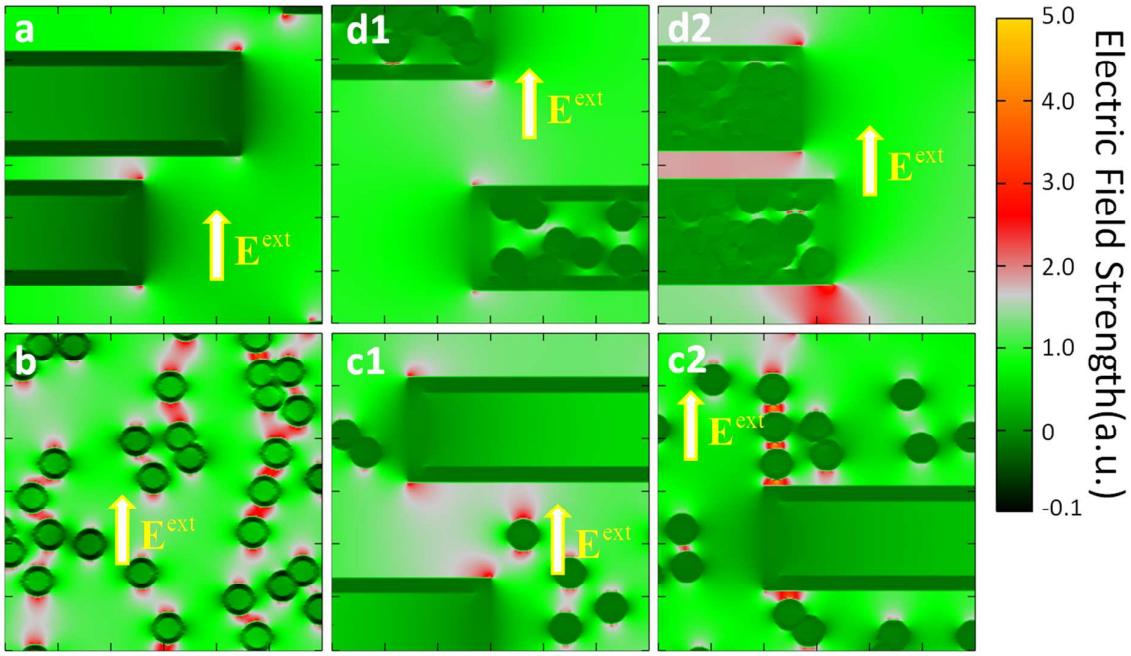

Figure 5

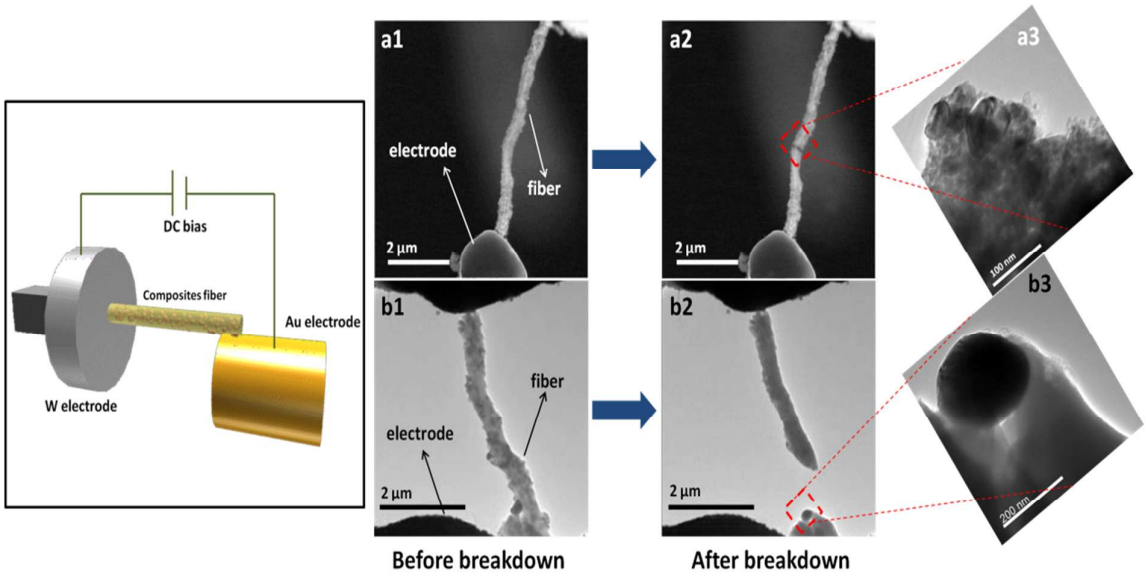

Figure 6

Hierarchical Interfaces Induce High-Dielectric –Permittivity of Nanocomposites Containing TiO_2@$BaTiO_3$ Nanofibers: Phase-Field Simulation and in-situ Observation of Electrical Breakdown by TEM

Xin Zhang[1], Weiwei Chen[1], Jianjun Wang[1], Yang Shen*[1], L. Gu[2], Yuanhua Lin[1], and Ce-Wen Nan*[1]

1 School of Materials Science and Engineering, State Key Lab of New Ceramics and Fine Processing, Tsinghua University Beijing, 100084, China.

2 *Chinese Academy of Science, Institute of Physics, Beijing National Lab of Condensed Matter Physics, POB 603, Beijing 100190, China.*

E-mail: shyang_mse@tsinghua.edu.cn; cwnan@tsinghua.edu.cn

TiO_2 nanofibers embedded with $BaTiO_3$ nanoparticles are fused with polyvinyl difluoride into polymer nanocomposites films. The hierarchical interfaces in the nanofibers induce a three-fold enhancement in dielectric permittivity of the polymer nanocomposites, which is attributed to the enhanced interfacial polarization as indicated by the phase field simulation and in-situ electrical breakdown test with TEM.